Postbuckling Analysis of Variable Angle Tow Composite Plates

Zhangming Wu[a], Gangadharan Raju[a], Paul M Weaver[b]

[a]*Research Assistant, Advanced Composite Centre for Innovation and Science, Department of Aerospace Engineering, Queen's Building, University Walk. United Kingdom*

[b]*Professor in Lightweight Structures, Advanced Composite Centre for Innovation and Science, Department of Aerospace Engineering, Queen's Building, University Walk. United Kingdom*

Abstract

Variable angle tow (VAT) placement techniques provide the designer with the ability to tailor the point-wise stiffness properties of composite laminates according to structural design requirements. Whilst VAT laminates exhibiting substantial gains in buckling performance have been shown previously, beneficial ways of using VAT techniques to improve structural performance of composite laminates in the postbuckling regime remain unclear. In the present study, a semi-analytical formulation based on a variational approach is developed and the Rayleigh-Ritz method is subsequently applied to solve the postbuckling problem of VAT plates. The generality of the proposed formulation allows effective modelling of the pure or mixed stress boundary conditions and also provides a computationally efficient means to determine the postbuckling strength of VAT plates. The proposed methodology is applied to the postbuckling problem of simply supported VAT plates under uni-

*Corresponding author

Email address: paul.weaver@bristol.ac.uk (Paul M Weaver)

form edge displacement compression. To show the accuracy and robustness of the proposed approach, results are validated using finite element analysis. The postbuckling characteristics of VAT plates subject to different in-plane boundary conditions are analysed by studying their nonlinear load-end shortening and transverse deflection responses. Furthermore, a parametric study on the postbuckling response of VAT plates with linear variation of fibre angle is performed and the stiffness values of VAT plates in both pre- and postbuckling ranges are compared with the results of straight-fibre laminates.
Keywords: Postbuckling, Variable Angle Tow, Rectangular Plates, Composite, Laminates

1. Introduction

Advanced tow placement techniques enable manufacture of steered fibre paths and so facilitate the synthesis of variable stiffness composite plates. In doing so, they provide additional freedom for structural tailoring opportunities. Previous works on variable stiffness laminates focused mainly on initial buckling and report an increase in critical buckling load by re-distribution of the prebuckling stresses (Gürdal et al., 2008; Wu et al., 2012c). However, very few works (Rahman et al., 2011) have been reported on the study of postbuckling behaviour of VAT laminates, and where they exist, rely substantially on finite element modelling, which requires significant computational efforts in solving the nonlinear postbuckling problem. There remains an ongoing need for rapid design tools which allow optimisation studies and provide physical insight into the fundamental behaviour which is not always readily achievable using commercial finite element analysis (FEA).

In aerospace applications, thin plate-like composite structures are widely used and often undergo large transverse deflections and have to carry considerable load beyond the buckling limit (Stein, 1959). Therefore, the load-carrying capacity, or, on the other hand, the weight-savings in the design of laminated composite plates can be further developed by studying their postbuckling behaviour. In this paper, an efficient approach based on a variational principle is proposed to solve the postbuckling problem of VAT laminates with linear fibre angle variation and the results are then analysed for a better understanding of their postbuckling behaviour.

In the study of postbuckling behaviour of a plate undergoing large deflections, the stretching of the middle surface of the plate due to out of plane displacement should be considered (Levy, 1945). The fundamental nonlinear strain-displacement relations and the partial differential equations for the large deflection of thin plates were derived by von Kármán. Based on von Kármán formulae, numerous works on the development of analytical methods have been proposed to study the postbuckling behaviour of plates. These methods were investigated in this work to ascertain their suitability for the postbuckling analysis of variable stiffness plates. The approximate postbuckling solution for an isotropic plate under longitudinal compression was obtained first by Marguerre (1937). He derived an expression for Airy's stress function written in terms of the unknown coefficients of out-of-plane deflection function from the compatibility equation. Then, the energy formula can be represented solely in terms of the assumed deflection function and a closed-form solution was achieved through minimising the total potential energy. Later, Levy (1945) obtained more accurate solutions by ex-

panding the stress function and the out-of-plane deflection function in terms of independent Fourier series. In his work, the general expressions for the stress coefficients in terms of deflection coefficients were derived from the compatibility equation. These expressions were then substituted into the nonlinear equilibrium equation to solve the postbuckling problem and also have been widely used in later published works (Coan, 1950; Yamaki, 1959; Chia, 1980; Shin et al., 1993). Coan (1950) extended Levy's work to plates with stress-free edges (mixed boundary conditions). Yamaki (1959) presented the analytical results of the isotropic plates with different boundary conditions. Prabhakara and Chia (1973) proposed a postbuckling analysis for orthotropic laminated composite plates under biaxial loading by using the Galerkin method and beam eigenfunctions. Shin et al. (1993) developed a model based on Marguerre's method for the postbuckling analysis of orthotropic laminates under uniform displacement compression. Harris (1975) proposed closed-form expressions for the evaluation of initial postbuckling stiffness using the principle of virtual work. Diaconu and Weaver (2005, 2006) derived approximate closed-form solution for postbuckling analysis of infinitely long composite plates under axial compression. The postbuckling problem was also solved by minimising the potential energy expressed in terms of three unknown displacement variables and considering the nonlinear von Kármán strain-displacement relationship (Feng, 1983; Sherbourne and Bedair, 1993; Seresta et al., 2005). Other works considering the effect of anisotropic coupling terms on the postbuckling analysis of composite laminates can be found in (Chia and Prabhakara, 1974; Harris, 1975; Zhang, 1982).

In previous works, the Rayleigh-Ritz energy method was shown to offer a concise and efficient way to analyse the behaviour of VAT composite plates. Alhajahmad et al. (2008, 2010) considered variable stiffness design tailoring for the nonlinear pressure-pillowing problem of fuselage skin panels based on the Rayleigh-Ritz energy method. Wu et al. (2012c) proposed an energy modelling combined using Airy's stress function for the prebuckling and buckling analysis of VAT plates. Airy's stress function is much more convenient for dealing with various in-plane boundary conditions than using the displacement functions, especially for the mixed (stress and displacement) boundary conditions. For the postbuckling analysis of VAT plates using the potential energy method, the closed-form solution (Levy, 1945; Coan, 1950; Yamaki, 1959; Shin et al., 1993) for Airy's stress function is obtained first. This, is found in terms of out of plane displacement, from the compatibility equation prior to the application of minimisation of the potential energy to find out of plane displacement. Due to the additional terms involving the derivatives of stiffness in the compatibility equation of variable stiffness plates, obtaining the Levy-type analytical closed-form solutions is generally difficult to find. Instead of solving the compatibility equation separately, this paper presents a semi-analytical approach using a single variational equation to derive the postbuckling solutions for VAT plates. Previously, Bisagni and Vescovini (2009a) applied this single variational formula to perform the postbuckling analysis of constant stiffness composite laminates with stiffeners. The advantages of using this variational formula to model the postbuckled VAT laminates are not only that the derivative terms of stiffness can be avoided, but that the compatibility equation, equilibrium equation and boundary con-

ditions (both for the prescribed displacements and stresses) can be treated simultaneously. The Rayleigh-Ritz (RR) method is then applied to minimise the variational formulae resulting in a system of nonlinear algebraic equations. The postbuckling equilibrium paths are traced from the derived nonlinear algebraic equations using an improved Newton-Raphson procedure. Legendre polynomials were used to achieve fast convergence and robustness in modelling the effects of flexural-twist anisotropy on postbuckling behaviour.

The content of this paper is arranged as follows. In the next section, the concept of VAT laminates and the definition for the variation of fibre-angle orientation are introduced. Section 3 presents the basic formulae for the postbuckling analysis of VAT plates, including the nonlinear governing equations, the potential energy and the variational principle. In section 4, the postbuckling model for VAT laminates under uniform displacement edge compression is implemented using the single variational form and the effects of in-plane boundary conditions on postbuckling responses of VAT plates are discussed. In section 5, the nonlinear load-end shortening curves and load-transverse deflection curves for square simply-supported VAT plates are determined and validated with FEA. In this study, the potential for exploiting the variable stiffness concept for enhanced postbuckling performance of composite laminates is investigated.

2. VAT Laminates

The terminology - Variable Angle Tow (VAT) refers to composite laminates that consist of plies with continuously variable in-plane fibre orientations, and as a result, their stiffness properties are also continuously changing

as functions of $x - y$ coordinates. The variable fibre orientation or the fibre trajectories of a VAT lamina are usually represented in a mathematical form using few fibre angle parameters. In previous work (Wu et al., 2012c), a general mathematical description for the variation of fibre angles was proposed. In this definition, a smooth distribution of fibre angles is defined using Lagrangian polynomials to interpolate the fibre angles at a set of pre-selected control points. In this paper, for the sake of simplicity, only the linear variation of fibre angle orientation is considered for the postbuckling analysis of VAT plates. The linear fibre angle variation, originally proposed by Gürdal and Olmedo (1993), is expressed as,

$$\theta(x) = \phi + \frac{2(T_1 - T_0)}{a}|x| + T_0 \tag{1}$$

where T_0 is the fibre orientation angle at the panel centre $x = 0$, T_1 is the fibre orientation angle at the panel ends $x = \pm a/2$ (as shown in Fig. 1) and ϕ is the angle of rotation of the fibre path.

Assuming the VAT plate is thin and applying classical lamination plate theory (CLPT), the constitutive equations for VAT plates in a partially inverted form is given by (Mansfield, 1989)

$$\begin{pmatrix} \epsilon^0 \\ \mathbf{M} \end{pmatrix} = \begin{bmatrix} \mathbf{a}(\mathbf{x},\mathbf{y}) & \mathbf{b}(\mathbf{x},\mathbf{y}) \\ -\mathbf{b^T}(\mathbf{x},\mathbf{y}) & \mathbf{D}^*(\mathbf{x},\mathbf{y}) \end{bmatrix} \begin{pmatrix} \mathbf{N} \\ \kappa \end{pmatrix} \tag{2}$$

where $\mathbf{a} = \mathbf{A^{-1}}$, $\mathbf{b} = -\mathbf{A^{-1}B}$, $\mathbf{D}^* = \mathbf{D} - \mathbf{BA^{-1}B}$ and $\mathbf{A}$, $\mathbf{B}$ and $\mathbf{D}$ are in-plane, coupling and bending stiffness matrices, respectively. For VAT plates, their values vary with the coordinates x and y. The term ϵ^0 is the mid-plane strains, κ is the curvature and $\mathbf{N}$, $\mathbf{M}$ are in-plane stress and bending moment resultants, respectively. As the VAT plates studied in this paper are

symmetrically laminated, there is no bending-stretching coupling and the coupling matrix $\mathbf{B} = 0$, $\mathbf{b} = 0$ and $\mathbf{D}^* = \mathbf{D}$.

3. Fundamental Theory

3.1. Governing equations

The von Kármán large deflection equations that define the nonlinear relation between the mid-plane strains and mid-plane displacements are (Bulson, 1970),

$$\begin{aligned} \epsilon_x^0 &= \frac{\partial u_0}{\partial x} + \frac{1}{2}\left(\frac{\partial w}{\partial x}\right)^2 \\ \epsilon_y^0 &= \frac{\partial v_0}{\partial y} + \frac{1}{2}\left(\frac{\partial w}{\partial y}\right)^2 \\ \gamma_{xy}^0 &= \frac{\partial u_0}{\partial x} + \frac{\partial v_0}{\partial y} + \left(\frac{\partial w}{\partial x}\right)\left(\frac{\partial w}{\partial y}\right) \end{aligned} \tag{3}$$

Applying Eq. (3) on *the condition of compatibility* leads to the relation,

$$\frac{\partial^2 \epsilon_x^0}{\partial y^2} + \frac{\partial^2 \epsilon_y^0}{\partial x^2} - \frac{\partial^2 \gamma_{xy}^0}{\partial x \partial y} = \left(\frac{\partial^2 w}{\partial x \partial y}\right)^2 - \frac{\partial^2 w}{\partial x^2}\frac{\partial^2 w}{\partial y^2} \tag{4}$$

From the constitutive equation of VAT laminates (Eq. (2)), the relation between mid-plane strains and the stress resultants $\mathbf{N}$ are given by,

$$\begin{aligned} \epsilon_x^0 &= a_{11}(x,y)N_x + a_{12}(x,y)N_y + a_{16}(x,y)N_{xy} \\ \epsilon_y^0 &= a_{12}(x,y)N_x + a_{22}(x,y)N_y + a_{26}(x,y)N_{xy} \\ \gamma_{xy}^0 &= a_{16}(x,y)N_x + a_{26}(x,y)N_y + a_{66}(x,y)N_{xy} \end{aligned} \tag{5}$$

The stretching behaviour of a plate can be modelled by introducing the Airy's stress function(Φ) and the stress resultants $\mathbf{N}$ (N_x, N_y, N_{xy}) are defined as,

$$N_x = \Phi_{,yy}, \quad N_y = \Phi_{,xx}, \quad N_{xy} = -\Phi_{,xy} \tag{6}$$

Substituting Eq. (5) and (6) into Eq. (4), the nonlinear compatibility equation expressed in terms of Airy's stress function for a VAT plate is given by,

$$\begin{aligned}
&\frac{\partial^2}{\partial y^2}\left[a_{11}(x,y)\Phi_{,yy} + a_{12}(x,y)\Phi_{,xx} - a_{16}(x,y)\Phi_{,xy}\right] + \\
&\frac{\partial^2}{\partial x^2}\left[a_{12}(x,y)\Phi_{,yy} + a_{22}(x,y)\Phi_{,xx} - a_{26}(x,y)\Phi_{,xy}\right] - \\
&\frac{\partial^2}{\partial x \partial y}\left[a_{16}(x,y)\Phi_{,yy} + a_{26}(x,y)\Phi_{,xx} - a_{66}(x,y)\Phi_{,xy}\right] = \\
&\qquad\qquad (w_{,xy})^2 - (w_{,xx})(w_{,yy})
\end{aligned} \tag{7}$$

Similarly, the nonlinear equilibrium equation for the large deflection of VAT plates is expressed by,

$$\begin{aligned}
&\frac{\partial^2}{\partial x^2}\left[D_{11}(x,y)w_{,xx} + D_{12}(x,y)w_{,yy} + 2D_{16}(x,y)w_{,xy}\right] + \\
&\frac{\partial^2}{\partial y^2}\left[D_{12}(x,y)w_{,xx} + D_{22}(x,y)w_{,yy} + 2D_{26}(x,y)w_{,xy}\right] + \\
&2\frac{\partial^2}{\partial x \partial y}\left[D_{16}(x,y)w_{,xx} + D_{26}(x,y)w_{,yy} + 2D_{66}(x,y)w_{,xy}\right] + \\
&\qquad\qquad \Phi_{,yy}w_{,xx} + \Phi_{,xx}w_{,yy} - 2\Phi_{,xy}w_{,xy} = 0
\end{aligned} \tag{8}$$

Expanding the derivatives in Eqs. (7) and (8), it was found that both the compatibility function and equilibrium equation for VAT laminates involve additional higher order derivative terms with respect to the in-plane flexibility and bending stiffness coefficients (a_{ij}, D_{ij}) (Gürdal and Olmedo, 1993; Gürdal et al., 2008; Raju et al., 2012), respectively. One may directly solve these two coupled governing equations by applying the Galerkin method (Prabhakara and Chia, 1973) or the principle of virtual work (displacement) (Harris, 1975; Pandey and Sherbourne, 1993) to determine the postbuckling behaviour of VAT plates, but is a tedious procedure. Other methods such as

DQM (Differential Quadrature Method) (Raju et al., 2012) or FDM (Finite Difference Method) may be applied to Eqs. (7) and (8) to obtain numerical solutions.

3.2. Variational principle

The distinct advantages of applying the energy method or a variational formulation to model the behaviour of VAT laminate are that the derivative terms of stiffness coefficients are avoided, and this leads to the analysis procedure for a VAT laminate analogous to a constant stiffness laminate. For example, the nonlinear von Kármán plate deflection problem is solved through minimising the strain energy or potential energy, which are expressed in terms of three unknown displacement fields (u, v, w) (Feng, 1983). This approach was used to solve the nonlinear problem of the pressure-loaded variable stiffness plates (Alhajahmad et al., 2008), as well as the postbuckling problem of the constant-stiffness plates (Feng, 1983; Sherbourne and Bedair, 1993; Seresta et al., 2005). The limitation of applying this method for the postbuckling analysis of VAT laminates is in the treatment of mixed boundary conditions. For instance, the displacement along a stress-free boundary is generally unknown and difficult to determine (Wu et al., 2012c).

In this work, a single variational formula expressed in terms of Airy's stress function and transverse deflection function is proposed to model the postbuckling behaviour of a VAT plate, which is defined by (Washizu, 1975; Bisagni and Vescovini, 2009a,b),

$$\begin{aligned}\mathbf{\Pi}^{*} = &-\frac{1}{2}\int \mathbf{N^{T}aN} + \frac{1}{2}\int \mathbf{k^{T}Dk} \\ &+ \int_{c_2} \left[u_0 N_{x\nu} + v_0 N_{y\nu}\right] ds\end{aligned} \tag{9}$$

$$\begin{aligned}\mathbf{\Pi}^{*} = &-\frac{1}{2}\iint_{S}\left[a_{11}(x,y)\left(\frac{\partial^2\Phi}{\partial y^2}\right)^2 + 2a_{12}(x,y)\frac{\partial^2\Phi}{\partial x^2}\frac{\partial^2\Phi}{\partial y^2} + a_{22}(x,y)\left(\frac{\partial^2\Phi}{\partial x^2}\right)^2\right. \\ &\left. + a_{66}(x,y)\left(\frac{\partial^2\Phi}{\partial x\partial y}\right)^2 - 2a_{16}(x,y)\frac{\partial^2\Phi}{\partial y^2}\frac{\partial^2\Phi}{\partial x\partial y} - 2a_{26}(x,y)\frac{\partial^2\Phi}{\partial x^2}\frac{\partial^2\Phi}{\partial x\partial y}\right]dxdy \\ &+ \frac{1}{2}\iint_{S}\left[D_{11}(x,y)\left(\frac{\partial^2 w}{\partial x^2}\right)^2 + 2D_{12}(x,y)\frac{\partial^2 w}{\partial x^2}\frac{\partial^2 w}{\partial y^2} + D_{22}(x,y)\left(\frac{\partial^2 w}{\partial y^2}\right)^2\right. \\ &\left. + 4D_{66}(x,y)\left(\frac{\partial^2 w}{\partial x\partial y}\right)^2 + 4D_{16}(x,y)\frac{\partial^2 w}{\partial x^2}\frac{\partial^2 w}{\partial x\partial y} + 4D_{26}(x,y)\frac{\partial^2 w}{\partial y^2}\frac{\partial^2 w}{\partial x\partial y}\right]dxdy \\ &+ \frac{1}{2}\iint_{S}\left[\frac{\partial^2\Phi}{\partial y^2}\left(\frac{\partial w}{\partial x}\right)^2 + \frac{\partial^2\Phi}{\partial x^2}\left(\frac{\partial w}{\partial y}\right)^2 - 2\frac{\partial^2\Phi}{\partial x\partial y}\frac{\partial w}{\partial x}\frac{\partial w}{\partial y}\right]dxdy \\ &+ \int_{c_1}\left[M_{\nu 0}\frac{\partial w}{\partial \nu} - \left(V_{z0} + \frac{\partial M_{\nu s0}}{\partial s}\right)w\right]ds + \int_{c_2}\left[u_0 N_{x\nu} + v_0 N_{y\nu}\right]ds\end{aligned} \tag{10}$$

where c_1 and c_2 denote the portion of boundaries over which stresses and displacements are prescribed, respectively. The descriptors s and ν indicate the tangential and normal direction respectively, along a specified boundary. Note, the boundary integrals ($\int_{c_1}, \int_{c_2}$) are important considerations to model various mixed boundary conditions, accurately. The geometric imperfection function of the VAT plate is included by adding the following integral term into the functional $\mathbf{\Pi}^{*}$ (Bisagni and Vescovini, 2009a),

$$\tilde{\mathbf{\Pi}}^{*} = \mathbf{\Pi}^{*} - \iint_{S}\left[\frac{\partial^2\Phi}{\partial y^2}\left(w_0\frac{\partial^2 w}{\partial x^2}\right) + \frac{\partial^2\Phi}{\partial x^2}\left(w_0\frac{\partial^2 w}{\partial y^2}\right) - \frac{\partial^2\Phi}{\partial xy}\left(w_0\frac{\partial^2 w}{\partial x\partial y}\right)\right]dxdy \tag{11}$$

where $w_0(x, y)$ is the function that represents initial imperfection shape.

Instead of solving the compatibility equation separately, the nonlinear strain-displacement relation can be included in the potential energy formula (Shin et al., 1993) by using the method of Lagrangian multipliers (Budiansky and Hu, 1946; Washizu, 1975; Wu et al., 2012a). After determining the Lagrangian multipliers explicitly and eliminating the unwanted variables, a single variational formula in terms of Airy's stress function and transverse deflection function, namely Eq. (10) is achieved. More details of the derivation can be found in a theoretical work regarding the complementary energy of thin plates with large deflection (Wang, 1952) and Washizu's variational principle (Washizu, 1975). From the stationary condition of the functional $\mathbf{\Pi}^*$, the nonlinear equilibrium equation, the compatibility equations and the prescribed moment and transverse shear stress resultants (out-of-plane) and displacement (in-plane) boundary conditions are satisfied. In addition, the in-plane stress and the out-of-plane displacement boundary conditions are satisfied either through the choice of the stress and deflection functions (Φ, w) (Wu et al., 2012c) or by applying additional Lagrangian multipliers (Wu et al., 2012b).

4. Postbuckling Model

4.1. Model implementation

The coordinate system (x, y) used in the functional $\mathbf{\Pi}^*$, for the sake of convenience, is normalised ($\xi = 2x/a, \eta = 2y/b, \quad \xi, \eta \in [-1, 1]$) in the analysis. To apply the Rayleigh-Ritz method, the transverse deflection function

w and Airy's stress function Φ are assumed to have the series forms,

$$w(\xi,\eta) = \sum_{r=0}^{R}\sum_{s=0}^{S} W_{rs} X_r(\xi) Y_s(\eta) \tag{12}$$

$$\Phi(\xi,\eta) = \Phi_0(\xi,\eta) + \sum_{p=0}^{P}\sum_{q=0}^{Q} \phi_{pq} X_p(\xi) Y_q(\eta) \tag{13}$$

where X_r, Y_s, X_p, Y_q are admissible functions that satisfy the given boundary conditions. For the simply-supported plate, $X_r(x), Y_s(y)$ are assumed to be either,

$$X_r(\xi) = \cos(\frac{r\pi\xi}{2}), \;\; Y_s(\eta) = \cos(\frac{s\pi\eta}{2}), \;\; m,n = 1,3,5,\cdots \tag{14}$$

using trigonometric functions, or

$$X_r(\xi) = (1-\xi^2)L_r(\xi), \;\; Y_s(\eta) = (1-\eta^2)L_s(\eta) \tag{15}$$

using Legendre polynomials. Note, in previous work (Wu et al., 2012a), Legendre polynomials had demonstrated superior convergence rates for the buckling analysis of laminated plates with high flexural-twisting anisotropy.

The options for the admissible functions $X_p(\xi), Y_q(\eta)$ and $\Phi_0(\xi,\eta)$ in Eq. (13) need to consider in-plane boundary conditions and the corresponding in-plane stress states. Three different in-plane boundary conditions for VAT plates under uniaxial compression are studied (Gürdal and Olmedo, 1993), which are illustrated in Figure 1. The VAT plate is subjected to uniform displacement compression ($x = \pm\frac{a}{2}$:$u = \mp\frac{\Delta_x}{2}$), and in *case A*, the transverse edges are free to deform; and in *case B*, the transverse edges are constrained, and in *case C*, the transverse edges are free to move but remain straight.

It has been shown previously that, under uniform displacement compression, the resultant boundary stress and the in-plane domain stresses of a VAT

plate are highly non-uniform in the prebuckling state (Gürdal et al., 2008; Wu et al., 2012c). On the other hand, in the postbuckling range, the stress distributions of plates (even an isotropic plate) are generally non-uniform (Coan, 1950) due to the nonlinear strain-displacement relation. For a VAT plate undergoing large deflection, both the variable stiffness and the nonlinear deflection are responsible for the non-uniform stress distribution. Airy's stress function $\Phi(\xi,\eta)$, in Eq. (13), is split into two parts for representing the non-uniform stresses distribution in the postbuckling regime, and also to satisfy the in-plane stress boundary conditions. Assuming that no boundary shear stresses exist and extension-shear coupling is not present ($A_{16}=0, A_{26}=0$), the series expansion in Eq. (13) satisfies the stress-free condition on all four edges and the function $\Phi_0(\xi,\eta)$ denotes the stress distribution along each loaded edges.

The admissible functions $X_p(x), Y_q(y)$ may take the forms (Wu et al., 2012b),

$$X_p(\xi) = (1-\xi^2)^2 L_p(\xi), \quad Y_q(\eta) = (1-\eta^2)^2 L_q(\eta) \tag{16}$$

or alternatively the clamped beam functions,

$$\begin{aligned} X_p(\xi') &= \cosh(\alpha_p\xi') - \cos(\alpha_p\xi') - \beta_p\left(\sinh(\alpha_p\xi') - \sin(\alpha_p\xi')\right), \\ Y_q(\eta') &= \cosh(\alpha_q\eta') - \cos(\alpha_q\eta') - \beta_q\left(\sinh(\alpha_q\eta') - \sin(\alpha_q\eta')\right) \end{aligned} \tag{17}$$

where $\xi' = (\xi+1)/2,\ \eta' = (\eta+1)/2$. $\alpha_p(\alpha_q)$, $\beta_p(\beta_q)$ are constants given by,

$$\cos(\alpha_p)\cosh(\alpha_p) = 1, \ \ \beta_p = \frac{\cosh(\alpha_p - \cos(\alpha_p))}{\sinh(\alpha_p - \sin(\alpha_p))} \tag{18}$$

and Φ_0 represents the unknown normal stress distributions (N_{x0}, N_{y0}) along

the boundary edges and are expanded into a series form,

$$\begin{aligned}
&\Phi_0(\xi,\eta) = f_1(\xi) + f_2(\eta) \\
&x = \pm\frac{a}{2}(\xi = \pm 1): \quad N_{x0} = \frac{4}{b^4}\frac{\partial^2\Phi_0}{\partial\eta^2} = \frac{4}{b^4}f_2''(\eta) = \frac{4}{b^4}\sum_{l=0,1,2,\cdots}^{L} c_l\psi_l^c(\eta) \\
&y = \pm\frac{b}{2}(\eta = \pm 1): \quad N_{y0} = \frac{4}{a^4}\frac{\partial^2\Phi_0}{\partial\xi^2} = \frac{4}{a^4}f_1''(\xi) = \frac{4}{a^4}\sum_{l=0,1,2,\cdots}^{L} d_l\psi_l^d(\xi).
\end{aligned} \tag{19}$$

where c_l and d_l are undetermined coefficients for the boundary stress distribution. $\psi_l^c(\eta)$ and $\psi_l^d(\xi)$ are admissible functions. A given amount of displacement loading ($u_0|_{\xi=\pm1} = \mp\frac{\Delta_x}{2}$) is applied by combining the assumed boundary stress resultants and substituting into the boundary integral part of Eq. (10). In *case A*, the transverse edges are stress-free, therefore $N_{y0}, d_l \equiv 0$ and only the first series expansion in Eq. (19) is needed for $\Phi_0 = \Phi_0(\xi)$. In *case B*, the zero displacement condition for the constraint transverse edges $u_0, v_0|_{\eta=\pm1} = 0$ should be used in Eq. (10). In *case C*, the transverse edges are allowed to move but constrained to be straight, which models the practical case of transverse edges of a VAT plate attached to stiffeners (Gürdal and Olmedo, 1993). As the movement of transverse edges is passive and driven by in-plane stretching, the work done by the edge stresses must equal zero (Gürdal and Olmedo, 1993),

$$\int_{-1}^{1} N_{y0}(\eta)d\eta = 0 \tag{20}$$

If Legendre polynomials are used for the admissible function of $\psi_l^d(\xi)$, then $d_0 \equiv 0$ by substituting Eq. (19) into Eq. (20). It implies that *case C* can be simulated in a similar way to *case B* but the first term of the series expansion of N_{y0} needs to be eliminated. However, a simple trigonometric series has

often been employed for the stress function expansion to model the *case C*, expressed as (Levy, 1945; Yamaki, 1959; Bisagni and Vescovini, 2009a),

$$\Phi(\xi,\eta) = -\frac{\hat{N}_{x0}\eta^2}{2} + \sum_{p=0}^{P}\sum_{q=0}^{Q}\phi_{pq}\cos(p\pi\xi)\cos(q\pi\eta) \tag{21}$$

where $\hat{N}_{x0}$ is average boundary load. Based on our experience, Legendre polynomials require less terms to capture the high non-uniform stress fields for a postbuckled VAT laminate than the trigonometric series and, provide efficiency and robustness in the numerical simulation.

Substituting Eqs. (13-19) into Eq. (10) and applying the Rayleigh-Ritz method, a set of nonlinear algebraic equations are obtained and expressed in the following tensor form,

$$\begin{aligned}
&K_{pi}^{mm}\phi_p + K_{li}^{mc}c_l + K_{li}^{md}d_l + K_{rsi}^{mb}W_rW_s = 0\\
&K_{pi}^{cm}\phi_p + K_{li}^{cc}c_l + K_{li}^{cd}d_l + K_{rsi}^{cb}W_rW_s = F_i\\
&K_{pi}^{dm}\phi_p + K_{li}^{dc}c_l + K_{li}^{dd}d_l + K_{rsi}^{db}W_rW_s = 0\\
&K_{ri}^{bb}W_r - K_{rpi}^{bm}W_r\phi_p - K_{rli}^{bc}W_rc_l - K_{rli}^{bd}W_rd_l = 0
\end{aligned} \tag{22}$$

where $K_{pi}^{mm}, K_{li}^{mc}, \cdots$ represent various stiffness matrices for a plate in the postbuckled state. The letters (b, m, c, d) in the superscript of each stiffness matrix (K) denote bending, membrane, the boundaries of loaded edges and transverse edges, respectively. A combination of two letters represents coupling effects, for example, K_{rsi}^{mb} denotes the nonlinear coupling between stretching and bending. The explicit expressions of the elements in each matrix are listed in the Appendix. Note, W_r and W_s are the vectorized form of the coefficient matrix W_{rs} in Eq. (12), and ϕ_p is the vectorized form of the coefficient matrix ϕ_{pq} in Eqs. (13) and (19). By eliminating the nonlinear

terms of the first three groups of equations in (22), it reduces to a prebuckling model for the VAT plate(Wu et al., 2012b),

$$\begin{bmatrix} K_{pi}^{mm} & K_{li}^{mc} & K_{li}^{md} \\ K_{pi}^{cm} & K_{li}^{cc} & K_{li}^{cd} \\ K_{pi}^{dm} & K_{li}^{dc} & K_{li}^{dd} \end{bmatrix} \begin{bmatrix} \phi_p \\ c_l \\ d_l \end{bmatrix} = \begin{bmatrix} 0 \\ F_i \\ 0 \end{bmatrix} \tag{23}$$

Besides, the last set of equations in (22) represent the corresponding buckling problem if the stress resultants (ϕ_p, c_l, d_l) are given, as

$$\left\{[K^{bb}] - \lambda[K^{bm} + K^{bc} + K^{bc}]\right\}\{W\} = 0 \tag{24}$$

A numerical routine based on Eqs. (22)-(24) was implemented in MATLAB for the prebuckling, buckling and postbuckling analysis of VAT plates. Firstly, the values of each stiffness matrix in Eq. (22) are computed. The integrations in the stiffness matrices, such as K_{ri}^{bb},K_{pi}^{mm},K_{ki}^{mc},$\cdots$, contain the variable stiffness terms are evaluated numerically. Closed-form solutions are available for the other matrices (K_{rsi}^{mb},K_{rsi}^{cb},$\cdots$) that are independent of material properties. Next, the non-uniform prebuckling stress resultants are determined using Eq. (23) and substituting into the Eq. (24) to obtain the critical buckling load (displacement). Finally, a Newton-Raphson method is applied to solve the nonlinear algebraic equations and determine the postbuckling equilibrium paths for the VAT plates. In the Newton-Raphson method, the applied load (displacement) is subdivided into a series of small incremental load steps, and in each step, the unknown coefficients of the deflection function (W) and stress function (ϕ, c, d) are obtained by an iterative root-finding procedure. Note, the initial step sizes are usually required to be sufficienty small to ensure convergence. The Jacobian matrix of Eq. (22) is

derived analytically to improve the computational efficiency. If no geometric imperfection is considered, the postbuckling analysis starts directly from the critical buckling point, otherwise it needs to start from a unloaded state.

In order to improve the numerical stability, the Newton-Raphson method is modified by a line search algorithm, in which a scalar factor ρ ($0.05 < \rho < 1$) is introduced to scale the solution in each iterative step, that is $x_{k+1} = x_k + \rho\Delta x$. Other numerical tracing techniques will be investigated and applied to improve or replace the Newton-Raphson method in future work. Note, the analysis takes around 10 seconds using our MATLAB numerical routine to trace the postbuckling equilibrium path of VAT plate on a computer with 3GHz processor and 2G memory. This contrasts with commercial FEA code which typically takes more than 200 seconds to produce similar fidelity results. This enables us to perform the optimum postbuckling design of VAT plates using stochastic optimisation techniques such as genetic algorithms in hours, whilst similar analysis in commercial FEA would take the order of weeks.

4.2. Stiffness indices

To normalise the postbuckling solutions, we compare results against a homogeneous quasi-isotropic laminate. The equivalent Young's modulus E_{iso}, Poisson's ratio ν_{iso} and bending stiffness D_{iso} of the quasi-isotropic laminate are given by (Pandey and Sherbourne, 1993; Diaconu and Weaver, 2005),

$$D_{iso} = \frac{E_{iso}h^3}{12(1-\nu_{iso}^2)}, \quad \nu_{iso} = \frac{U_4}{U_1}, \quad E_{iso} = U_1(1-\nu_{iso}^2) \tag{25}$$

where U_1, U_2, U_4 are material invariants (Jones, 1998). The applied loads and end-shortening strains in the postbuckling curves are normalised with

respect to that of this quasi-isotropic laminate at its critical buckling state.

The postbuckling strength of a plate is often quantified, in a conventional way, by calculating the slope of the load-end shortening curve immediately after the buckling takes place (Bulson, 1970; Pandey and Sherbourne, 1993; Diaconu and Weaver, 2005). This quantity, namely the relative stiffness (denoted by K_r), reflects the proportion of stiffness that remains in the postbuckling regime against its initial prebuckling stiffness (K_{pre})(Diaconu and Weaver, 2005). The relative stiffness, however, does not convey any information regarding the configurations of laminates. In order to perform the layup comparison and consider the stiffness in both pre- and postbuckling regimes simultaneously, two other quantities are defined in this work to characterise the postbuckling behaviours of VAT laminates. One is the normalised postbuckling stiffness (K_{post}) (Pandey and Sherbourne, 1993), which is defined as the slope of the initial postbuckling range divided by the prebuckling stiffness (K_{iso}) of the quasi-isotropic laminate. The other is the normalised overall stiffness (K_o) that is directly quantised by the end-shortening strain (ϵ_x^o) under a certain load condition (N_x^o), which is often chosen to be in the range of one to three times the critical buckling load of the quasi-isotropic laminate (N_x^{iso}). In this work, possible mode jumping in the procedure of the postbuckling equilibrium paths is prevented. For the cases that the applied load is less than the prescribed value but mode jumping has occured, the resultant end-shortening strain is estimated by the initial postbuckling

slope. The formulae for calculating these stiffness indices are,

$$\begin{aligned} K_{pre} &= \frac{N_x^{cr}}{\epsilon_x^{cr}} = a\frac{N_x^{cr}}{\Delta_x^{cr}}, \quad K_r = \frac{1}{K_{pre}}\left(\frac{dN}{d\epsilon}\right)_{av} \\ K_{post} &= \frac{1}{K_{iso}}\left(\frac{dN}{d\epsilon}\right)_{av}, \quad K_o = \frac{1}{K_{iso}}\frac{N_x^o}{\epsilon_x^o} \end{aligned} \tag{26}$$

The closed-form solutions (Bulson, 1970; Pandey and Sherbourne, 1993) for the prebuckling stiffness (K_{iso}), critical buckling load (N_x^{iso}), the end-shortening strain (ϵ_x^{iso}) and the postbuckling relative stiffness (K_r) of a square isotropic plate subjected to an uniaxial compression and different in-plane boundary conditions that defined as *case A,B,C* in section 4 are provided in the following text.

For *case A*, that the unloaded edges are free to deform,

$$\begin{aligned} K_{iso} &= E_{iso}h, \quad N_x^{iso} = \frac{4\pi^2 D_{iso}}{b^2}, \quad \epsilon_x^{iso} = \frac{N_x^{cr}}{K_{iso}}, \\ K_r &= \frac{1}{K_{iso}}\frac{dN}{d\epsilon} = 0.408 \end{aligned} \tag{27}$$

For *case B*, that the unloaded edges are in-plane constrained,

$$\begin{aligned} K_{iso} &= \frac{E_{iso}h}{1-\nu_{iso}^2}, \quad N_x^{iso} = \frac{4\pi^2 D_{iso}}{b^2(1+\nu_{iso})}, \quad \epsilon_x^{iso} = \frac{N_x^{cr}}{K_{iso}} \\ K_r &= \frac{1}{K_{iso}}\frac{dN}{d\epsilon} = 0.56 \end{aligned} \tag{28}$$

For *case C*, that the unloaded edges are free to move but remain straight, the prebuckling stiffness and the critical buckling load (strain) are identical with *case A*. The relative postbuckling stiffness is well-known as $K_r = 0.5$, which is slightly higher than *case A* due to the presence of edge stiffeners.

5. Results and Discussion

5.1. Model validation and boundary effects

The postbuckling modelling results of VAT plates subjected to an uniform axial compression are presented in this section. Square VAT plates (a = b = 0.5 m) with 16 balanced, symmetric layup, linear variation of fibre-orientation angles ($[\phi \pm \langle T_0|T_1\rangle]_{4s}$) and all the plate edges simply-supported are investigated for the postbuckling model validation. Three different in-plane boundary conditions (*case A,B,C*) that are defined in section 4 are investigated. The lamina properties are given by $E_1 = 163$GPa, $E_2 = 6.8$GPa, $G_{12} = 3.4$GPa, ν_{12}= 0.28. Ply thickness is 0.13mm (the plate thickness is 2.1 mm).

Finite element modelling for the postbuckling analysis of VAT plates was carried out using ABAQUS and a subroutine was developed to generate ABAQUS composite elements with independent fibre orientations. The S4 shell element was chosen for discretization of the VAT plate structure and a mesh density of 40×40 was selected to achieve the required accuracy. Each finite element was assumed to have a constant fibre orientation in order to model the linear fibre angle distribution within each of the lamina. The thickness variation of the VAT plate due to tow overlap or gaps were not considered and the ply-thickness is assumed to be constant in the present study. A small imperfection in the form of the first buckling mode shape and a magnitude of 1% of the plate thickness is imposed to each finite element modelling.

Figures 2-4 show the postbuckling results of VAT composite plates compared with straight-fibre laminates for the *cases A, B* and *C*, respectively.

The results of both VAT laminates and straight-fibre laminates obtained by the Rayleigh-Ritz method correlate well with FEA. In the Rayleigh-Ritz method, sufficient number of polynomials for each admissible function was chosen to achieve converged results. For the simply-supported square plate problem, $R = 6, S = 6$ is chosen for the deflection function and $P = 4, Q = 4, K = 4$ for the Airy's stress function. The maximum transverse displacement w_{max} is normalised with respect to the plate thickness h. The average axial load N_x is normalised with the critical buckling load N_x^{iso} for a quasi-isotropic laminate. The strain ϵ_x is normalised with respect to ϵ_x^{iso}, which is the end shortening strain at critical buckling load for a quasi-isotropic laminate (Diaconu and Weaver, 2005).

Fig. 2-a shows the normalised load vs normalised axial end-shortening strain curves for *case A*. For the constant stiffness laminates, the maximum compressive stiffness is, obviously, given by a $[0]_{16}$ laminate, while $[\pm 45]_{4s}$ laminate has the maximum buckling load and very poor performance with respect to both the pre- and postbuckling stiffness. Three VAT laminates are selected for the comparison in Fig. 2-a. The $[90 \pm \langle 0|75 \rangle]_{4s}$ laminate has the highest buckling load among all the VAT configurations $[\phi \pm \langle T_0|T_1 \rangle]_{4s}$ with linear variation of fibre angles (Gürdal et al., 2008), however, its prebuckling and postbuckling axial stiffness is much lower than the quasi-isotropic and $[0]_{16}$ laminates. On the other hand, the relative postbuckling stiffness of the $[90 \pm \langle 0|75 \rangle]_{4s}$ VAT plate is relatively high ($K_r = 0.56$), which means there is less reduction of axial stiffness after entering the postbuckling regime. This is mainly because the majority of compressive load is redistributed towards the edges and the load redistribution due to the variable stiffness is still dominant

in the initial postbuckling regime. The VAT laminate $[90 \pm \langle 10|75 \rangle]_{4s}$ exhibits higher value of relative postbuckling stiffness $K_r = 0.71$ compared to other linear VAT configurations. VAT plate $[0 \pm \langle 0|15 \rangle]_{4s}$ exhibits the lowest end-shortening strain, in other words the highest overall stiffness, under a given load ($2N_{iso}$). Its prebuckling stiffness is almost the same as $[0]_{16}$ but the postbuckling stiffness is slightly improved. Fig. 2-b shows the normalised maximum transverse displacement w_{max}/h function vs the normalised axial load. The maximum transverse deflection for $[90 \pm \langle 0|75 \rangle]_{4s}$ VAT laminate is found to be much less than the other layups and this result demonstrates the considerable superiority of applying variable stiffness to restrict the maximum transverse deflection for a postbuckled laminated plate.

The postbuckling behaviour of plates under uniform compression with transverse edges constrained (*case B*) were studied and the results are shown in Fig. 3. The end-shortening curves in Fig. 3-a clearly show that both $[\pm 32]_{4s}$ and $[0 \pm \langle 0|50 \rangle]_{4s}$ laminate exhibit high buckling load, but perform poorly in the postbuckling regime. The fibre distribution of $[0 \pm \langle 0|50 \rangle]_{4s}$ laminate gives rise to no re-distribution of the axial compression load, and provides much less contribution to improve postbuckling stiffness. The VAT plate $[0 \pm \langle 0|20 \rangle]_{4s}$ exhibits higher prebuckling and postbuckling stiffness than the other $[\phi \pm \langle T_0|T_1 \rangle]_{4s}$ layups (Fig.3-a) and the $[0]_{16}$ laminate demonstrated high overall stiffness value when compared to VAT laminates. Fig. 3-b shows the nonlinear transverse deflection response of different laminates and the VAT plate $[90 \pm \langle 0|85 \rangle]_{4s}$ demonstrates the lowest maximum transverse displacement.

The structural responses of plates under the boundary condition of *case*

C are shown in Fig. 4, in which the results of *case A* are also presented (denoted by the dash-dot lines) for comparison purposes. For the boundary condition of *case C*, the prebuckling behaviour and the critical buckling state of the straight-fibre laminates and VAT plates with stiffness varying along y direction ($\theta(y)$) were observed to be identical to *case A* (Gürdal and Olmedo, 1993; Gürdal et al., 2008). The postbuckling behaviour (stiffness) of straight-fibre laminates under *case C* are generally bounded in between the results of *case A* and *case B* (Bulson, 1970). The effects of in-plane boundary conditions on the postbuckling responses of VAT laminates largely depend on the distributions of their variable stiffness. Three VAT plates are shown in Fig. 4-a to illustrate the differences raised by the boundary conditions of *case A* and *case C* on their postbuckling behaviour. The $[0 \pm \langle 0|20\rangle]_{4s}$ plate gives the highest overall stiffness among the VAT laminates with linear varation of fibre angles ($[\phi \pm \langle T_0|T_1\rangle]_{4s}$) for *case C*. Fig. 4-a shows that the postbuckling stiffness of quasi-isotropic, 0° and VAT layup $[0 \pm \langle 0|20\rangle]_{4s}$ under *case C* is slightly higher than the result for *case A*. The differences in the load-end shortening behavior between *case A* and *case C* are much less for the other two VAT plates $[90 \pm \langle 0|75\rangle]_{4s}$ and $[90 \pm \langle 10|75\rangle]_{4s}$. In particular, the solutions of the $[90 \pm \langle 0|75\rangle]_{4s}$ VAT laminate for *case C* are nearly the same as that of *case A*. The load-transverse deflection curves for these laminates are plotted in Fig. 4-b, which demonstrates the similar trends with the results shown in Fig. 2-b for *case A*.

In the manufacture of VAT laminated plates with shifted fibre paths using the tow-steered techniques, thickness variation is an inevitable consequence. Tows consist of multiple fibres which are free to slide over each other for dry

tow placement and deform in shear for towpreg techniques such as automatic fibre placement. As such, when a flat tow is curved, individual fibres slide to narrow the tow and minimise the excess length associated with outer radius compared with inner radius. In so doing, the tow thickens. Once all tows are laid down such thickness change manifests itself as a smooth variation across the plate (Kim et al., 2012). For example, the thickness along the transverse edges of the $[90 \pm \langle 0|75 \rangle]_{4s}$ VAT laminate or other analogous layups are likely to be increased due to the maximum change in shifting angle. From the simulation results, it was observed that such a thickness build-up further improve the postbuckling stiffness (relative stiffness) of these VAT laminates. This suggests that the thickness variation offers us an additional design parameter to perform the postbuckling design of VAT laminates. However, a thorough study of the effects of thickness variation on the postbuckling behaviour of VAT laminate is beyond the scope of the paper and, it will be investigated in the future works.

5.2. Parametric study

A parametric study of postbuckling behaviour of square VAT plates with linear variation of fibre angles is presented in this section. The postbuckling analysis were carried out on the VAT laminates by varying the fibre angles T_0 and T_1 (Eq. (1)) between 0° to 90° with a step of 5°. Only the variation of fibre angles (stiffness) along y direction ($[\pm\theta(y)]_{4s}$) is considered in this study, as these configurations demonstrate good buckling performance (Gürdal et al., 2008; IJsselmuiden et al., 2010; Wu et al., 2012c) for the three in-plane boundary conditions. The relative stiffness K_r, postbuckling stiffness K_{post}, the plate overall stiffness K_o and the critical buckling load

of the VAT plates under the boundary conditions of *case B* and *case C* are computed. The results for *case A* are not presented, as it has been discussed that this boundary case is similar to *case C*. The computed results $K_r, K_{post}, K_o, N_x^{cr}$ are normalised and shown in Figures 5 and 6 as functions of the normalised prebuckling stiffness for *case B* and *case C*, respectively. Each curve in the figures represent a series of VAT plates with various values of T_1 (from 0° at the left-end to 90° at the right-end), but with the same value of T_0, which is labeled in the figure. The red dash curve denotes the result of straight-fibre laminates which vary from $[90]_{16}$ to $[0]_{16}$ as one moves from left to right in each plot.

For *case B*, the largest relative stiffness shown in the Fig. 5-a is $K_r = 0.75$ and is achieved by the VAT configuration $[90 \pm \langle 0|25\rangle]_{4s}$, which is slightly more than the maximum value $K_r = 0.73$ given by the straight-fibre laminate $[\pm 65]_{4s}$. But the prebuckling stiffness of these two laminates are relatively low and results in poor behaviour of the overall stiffness. From Figs. 5-b and -c, the variation of postbuckling stiffness with respect to various VAT formats is very close to that describing the overall stiffness. The buckling performance of the VAT plates under *case B* is shown in Fig. 5-d. The $[90 \pm \langle 0|80\rangle]_{4s}$ has the maximum normalised buckling load (N_x^{cr}/N_x^{iso}) 1.40, which is 25% higher than the maximum value 1.12 obtained by a straight-fibre laminate $[\pm 30]_{4s}$. The $[0]_{16}$ laminate exhibits the highest prebuckling stiffness for the case of uniaxial compression and it also results in the largest postbuckling stiffness (overall stiffness) as shown in Figs. 5-b and -c. Nevertheless, if the VAT plate's normalised prebuckling stiffness K_{pre}/K_{iso} is restricted to 0.5 and 2, the stress redistribution caused by tow-steering is

significant and this phenomena is responsible for considerable improvement of the postbuckling responses. For prebuckling stiffness out of this range, the stress redistribution is primarily due to the von Kármán nonlinear strain-displacement relations governing the postbuckling behaviour. For instance, considering a VAT plate $[90 \pm \langle 20|90 \rangle]_{4s}$ and a straight-fibre laminate $[\pm 38]_{4s}$, both of them approximately have an equivalent prebuckling stiffness as the quasi-isotropic laminate ($K_{pre} = K_{iso}$). The relative stiffness, postbuckling stiffness, overall stiffness and buckling load of the VAT plate $[90 \pm \langle 20|90 \rangle]_{4s}$ show an improvement of 291%, 317%, 230% and 15% over the straight-fibre laminate $[\pm 38]_{4s}$, respectively.

The superiority of VAT laminates with respect to the postbuckling responses was also observed for *case C*, as shown in Fig. 6. The VAT plate $[90 \pm \langle 10|70 \rangle]_{4s}$ has the maximum relative stiffness $K_r = 0.72$ and exhibits 12% improvement over the maximum value 0.64 of a straight-fibre laminate $[\pm 55]_{4s}$. The sharp variation of postbuckling behaviour with small variations in linear fibre distribution, observed in Fig. (6)-a and -b, can be attributed to discrete changes in mode shape with associated similar buckling loads (Rahman et al., 2011). The buckling performance for this case is shown in Fig. 6-d, which is identical to the results shown in (Gürdal et al., 2008). Similar to *case B*, VAT configurations provide considerably improved postbuckling responses when the plate's normalised prebuckling stiffness is less than 2. It was concluded that load redistribution towards the supported edges is the primary mechanism for the improvement of postbuckling response. Therefore, Figs. 5 and 6 show that the VAT concept provides more flexibility in stiffness tailoring of the laminate configurations to achieve better postbuck-

ling performance.

6. Conclusion

In this work, a semi-analytical variational approach was developed to perform postbuckling analysis of VAT plates under uniform axial compression loading. The generality of the proposed approach was discussed and shown by modelling mixed stress/displacement boundary conditions. The different in-plane boundary conditions are implemented either using trigonometric functions or Legendre polynomials. The postbuckling solutions for each boundary condition are determined using the proposed approach and validated with FEA to show the good accuracy, robustness and efficiency of this proposed approach.

The load-end shortening curves and load-transverse deflection curves for the postbuckled VAT plates were computed and compared with the results of straight-fibre laminates. The effects of in-plane boundary conditions on the postbuckling behaviour of VAT plates are discussed. Subsequently, a parametric study on the postbuckling behaviour of VAT plates was shown with a linear fibre angle variation. In this study, the postbuckling stiffness, relative stiffness, overall plate stiffness and the critical buckling load are computed and plotted as functions of the normalised prebuckling stiffness. It is demonstrated that enhanced results are given by the VAT laminates, in which only small amounts of stiffness reduction occur in the postbuckling regime and simultaneously their overall stiffness and critical buckling load are maintained to be relatively high. From this study, the advantages of applying the variable stiffness concept for enhanced postbuckling performance of composite

laminates were demonstrated.

Acknowledgments

The authors wish to acknowledge EPSRC, Airbus and GKN for supporting this research under the project ABBSTRACT2 (EP/H025898/1).

Appendix

The explicit forms for the tensors in the postbuckling model (Eq. (22)) are expressed below. Each vectorized coefficient in Eq. (22) is reverted back to its matrix form, W_r or W_s to $W_{rs}(W_{\bar{r}\bar{s}})$ and ϕ_p to $\phi_{pq}(\phi_{\bar{p}\bar{q}})$ (For example, $W_0 = W_{00}, W_1 = W_{01}, W_2 = W_{02}, \cdots,$).

$$\begin{aligned} K_{pi}^{mm}(K_{pq\bar{p}\bar{q}}^{mm}) = \int_{-1}^{1}\int_{-1}^{1}\Big[&\mu^4 a_{11} X_p Y_{q,\eta\eta} X_{\bar{p}} Y_{\bar{q},\eta\eta} + \\ &\mu^2 a_{12}(X_p Y_{q,\eta\eta} X_{\bar{p},\xi\xi} Y_{\bar{q}} + X_{p,\xi\xi} Y_q X_{\bar{p}} Y_{\bar{q},\eta\eta}) + \\ &a_{22} X_{p,\xi\xi} Y_q X_{\bar{p},\xi\xi} Y_{\bar{q}} + \mu^2 a_{66} X_{p,\xi} Y_{q,\eta} X_{\bar{p},\xi} Y_{\bar{q},\eta} - \\ &\mu^3 a_{16}(X_{p,\xi} Y_{q,\eta} X_{\bar{p}} Y_{\bar{q},\eta\eta} + X_p Y_{q,\eta\eta} X_{\bar{p},\xi} Y_{\bar{q},\eta}) - \\ &\mu a_{26}(X_{p,\xi\xi} Y_q X_{\bar{p},\xi} Y_{\bar{q},\eta} + X_{p,\xi} Y_{q,\eta} X_{\bar{p},\xi\xi} Y_{\bar{q}})\Big] d\xi d\eta \end{aligned} \tag{29}$$

$$\begin{aligned} K_{li}^{mc}(K_{l\bar{p}\bar{q}}^{mc}) = \int_{-1}^{1}\int_{-1}^{1}\Big(&\mu^4 a_{11}\psi_l^c X_{\bar{p}} Y_{\bar{q},\eta\eta} + \mu^2 a_{12}\psi_l^c X_{\bar{p},\xi\xi} Y_{\bar{q}} - \\ &\mu^3 a_{16}\psi_l^c X_{\bar{p},\xi} Y_{\bar{q},\eta}\Big) d\xi d\eta \end{aligned} \tag{30}$$

$$\begin{aligned} K_{li}^{md}(K_{l\bar{p}\bar{q}}^{md}) = \int_{-1}^{1}\int_{-1}^{1}\Big(&\mu^2 a_{12}\psi_l^d X_{\bar{p}} Y_{\bar{q},\eta\eta} + a_{22}\psi_l^d X_{\bar{p},\xi\xi} Y_{\bar{q}} - \\ &\mu a_{26}\psi_l^d X_{\bar{p},\xi} Y_{\bar{q},\eta}\Big) d\xi d\eta \end{aligned} \tag{31}$$

$$K_{rsi}^{mb}(K_{rs\bar{r}\bar{s}\bar{p}\bar{q}}^{mb}) = \frac{1}{2}\mu^2 \int_{-1}^{1}\int_{-1}^{1}\Big(X_{r,\xi}Y_sX_{\bar{r},\xi}Y_{\bar{s}}X_{\bar{p}}Y_{\bar{q},\eta\eta} + X_rY_{s,\eta}X_{\bar{r}}Y_{\bar{s},\eta}X_{\bar{p},\xi\xi}Y_{\bar{q},\eta\eta} + X_{r,\xi}Y_sX_{\bar{r}}Y_{\bar{s},\eta}X_{\bar{p},\xi}Y_{\bar{q},\eta}\Big)d\xi d\eta \tag{32}$$

$$K_{li}^{cc}(K_{l\bar{l}}^{cc}) = \int_{-1}^{1}\int_{-1}^{1}\mu^4 a_{11}\psi_l^c\psi_{\bar{l}}^c d\xi d\eta \tag{33}$$

$$K_{li}^{cd}(K_{l\bar{l}}^{cd}) = \int_{-1}^{1}\int_{-1}^{1}\mu^2 a_{12}\psi_l^c\psi_{\bar{l}}^d d\xi d\eta \tag{34}$$

$$K_{rsi}^{cb}(K_{rs\bar{r}\bar{s}\bar{l}}^{cb}) = \frac{1}{2}\mu^2 \int_{-1}^{1}\int_{-1}^{1}X_{r,\xi}Y_sX_{\bar{r},\xi}Y_{\bar{s}}\psi_{\bar{l}}^c d\xi d\eta \tag{35}$$

$$K_{li}^{dd}(K_{l\bar{l}}^{dd}) = \int_{-1}^{1}\int_{-1}^{1}a_{22}\psi_l^d\psi_{\bar{l}}^d d\xi d\eta \tag{36}$$

$$K_{rsi}^{db}(K_{rs\bar{r}\bar{s}\bar{l}}^{db}) = \frac{1}{2}\mu^2 \int_{-1}^{1}\int_{-1}^{1}X_rY_{s,\eta}X_{\bar{r}}Y_{\bar{s},\eta}\psi_{\bar{l}}^d d\xi d\eta \tag{37}$$

$$\begin{aligned} K_{ri}^{bb}(K_{rs\bar{r}\bar{s}}^{bb}) = \int_{-1}^{1}\int_{-1}^{1}\Big[& D_{11}X_{r,\xi\xi}Y_sX_{\bar{r},\xi\xi}Y_{\bar{s}} \\ & + \mu^2 D_{12}(X_rY_{s,\eta\eta}X_{\bar{r},\xi\xi}Y_{\bar{s}} + X_{r,\xi\xi}Y_sX_{\bar{r}}Y_{\bar{s},\eta\eta}) \\ & + \mu^4 D_{22}X_rY_{s,\eta\eta}X_{\bar{r}}Y_{\bar{s},\eta\eta} + 4\mu^2 D_{66}X_{r,\xi}Y_{s,\eta}X_{\bar{r},\xi}Y_{\bar{s},\eta} \\ & + 2\mu D_{16}(X_{r,\xi}Y_{s,\eta}X_{\bar{r}}Y_{\bar{s},\eta\eta} + X_rY_{s,\eta\eta}X_{\bar{r},\xi}Y_{\bar{s},\eta\eta}) \\ & + 2\mu^3 D_{26}(X_{r,\xi\xi}Y_sX_{\bar{r},\xi}Y_{\bar{s},\eta} + X_{r,\xi}Y_{s,\eta}X_{\bar{r},\xi\xi}Y_{\bar{s}})\Big]d\xi d\eta \end{aligned} \tag{38}$$

$$K_{rli}^{bc}(K_{rsl\bar{r}\bar{s}}^{bc}) = \mu^2 \int_{-1}^{1}\int_{-1}^{1}X_{r,\xi}Y_s\psi_l^c X_{\bar{r},\xi}Y_{\bar{s}}d\xi d\eta \tag{39}$$

$$K_{rli}^{bd}(K_{rsl\bar{r}\bar{s}}^{bd}) = \mu^2 \int_{-1}^{1}\int_{-1}^{1}X_rY_{s,\eta}\psi_l^d X_{\bar{r}}Y_{\bar{s},\eta}d\xi d\eta \tag{40}$$

$$K_{pi}^{cm} = (K_{li}^{mc})^T, \quad K_{pi}^{dm} = (K_{li}^{md})^T, \quad K_{li}^{dc} = (K_{li}^{cd})^T \tag{41}$$

where $r, \bar{r} = 0, 1, 2, \cdots, R,\ s, \bar{s} = 0, 1, 2, \cdots, S,\ p, \bar{p} = 0, 1, 2, \cdots, P,\ q, \bar{q} = 0, 1, 2, \cdots, Q,\ l, \bar{l} = 0, 1, 2, \cdots, L$.

References

Alhajahmad, A., Abdalla, M. M., Gürdal, Z., 2010. Optimal design of tow-placed fuselage panels for maximum strength with buckling considerations. Journal of Aircraft 47 (3), 775 – 782.

Alhajahmad, A., Abdallah, M. M., Gürdal, Z., 2008. Design tailoring for pressure pillowing using tow-placed steered fibers. Journal of Aircraft 45 (2), 630 – 640.

Bisagni, C., Vescovini, R., 2009a. Analytical formulation for local buckling and post-buckling analysis of stiffened laminated panels. Thin-Walled Structures 47 (3), 318 – 334.

Bisagni, C., Vescovini, R., 2009b. Fast tool for buckling analysis and optimization of stiffened panels. Journal of Aircraft 46 (6), 2041 – 2053.

Budiansky, B., Hu, P. C., 1946. The lagrangian multiplier method of finding upper and lower limits to critical stresses of clamped plates. NACA, Report No. 848.

Bulson, P. S., 1970. The Stability of Flat Plates. Chatto and Windus Ltd, London.

Chia, C., Prabhakara, M., 1974. Postbuckling behavior of unsymmetrically layered anisotropic rectangular plates. Journal of Applied Mechanics, Transactions ASME 41 Ser E (1), 155 – 162.

Chia, C.-Y., 1980. Nonlinear Analysis of Plates. McGraw-Hill International Book Company.

Coan, J. M., 1950. Large deflection theory for plates with small initial curvature loaded in edge compression. Journal of Applied Mechanics 18, 143–151.

Diaconu, C. G., Weaver, P. M., 2005. Approximate solution and optimum design of compression-loaded, postbuckled laminated composite plates. AIAA Journal 43 (4), 906 – 914.

Diaconu, C. G., Weaver, P. M., 2006. Postbuckling of long unsymmetrically laminated composite plates under axial compression. International Journal of Solids and Structures 43 (22-23), 6978–6997.

Feng, M., 1983. An energy theory for postbuckling of composite plates under combined loading. Computers and Structures 16 (14), 423 – 431.

Gürdal, Z., Olmedo, R., 1993. In-plane response of laminates with spatially varying fiber orientations. variable stiffness concept. AIAA journal 31 (4), 751 – 758.

Gürdal, Z., Tatting, B., Wu, C., 2008. Variable stiffness composite panels: Effects of stiffness variation on the in-plane and buckling response. Composites Part A: Applied Science and Manufacturing 39 (5), 911 – 922.

Harris, G., 1975. The buckling and post-buckling behaviour of composite plates under biaxial loading. International Journal of Mechanical Sciences 17 (3), 187 – 202.

IJsselmuiden, S. T., Abdalla, M. M., Gürdal, Z., 2010. Optimization of variable-stiffness panels for maximum buckling load using lamination parameters. AIAA Journal 48 (1), 134 – 143.

Jones, R. M., 1998. Mechanics of composite materials. CRC Press, 2nd Revised edition edition.

Kim, B. C., Potter, K., Weaver, P. M., 2012. Continuous tow shearing for manufacturing variable angle tow composites. Composites Part A: Applied Science and Manufacturing 43 (8), 1347 – 1356.

Levy, S., 1945. Bending of rectangular plates with large deflections. NACA, Report No. 737.

Mansfield, E. H., 1989. The bending and stretching of plates, Second Edition. Cambridge University Press.

Marguerre, K., 1937. The apparent width of the plate in compression. NACA, Report No. 833.

Pandey, M., Sherbourne, A., 1993. Postbuckling behaviour of optimized rectangular composite laminates. Composite Structures 23 (1), 27 – 38.

Prabhakara, M. K., Chia, C. Y., 1973. Post-buckling behaviour of rectangular orthotropic plates. Journal of Mechanical Engineering Science 15 (1), 25–33.

Rahman, T., Ijsselmuiden, S. T., Abdalla, M. M., Jansen, E. L., 2011. Postbuckling analysis of variable stiffness composite plates using a finite element-based perturbation method. International Journal of Structural Stability and Dynamics 11 (04), 735–753.

Raju, G., Wu, Z., Kim, B. C., Weaver, P. M., 2012. Prebuckling and buckling

analysis of variable angle tow plates with general boundary conditions. Composite Structures 94 (9), 2961 – 2970.

Seresta, O., Abdalla, M. M., Gürdal, Z., 2005. Optimal design of laminated composite plates for maximum post buckling strength. Collection of Technical Papers - AIAA/ASME/ASCE/AHS/ASC Structures, Structural Dynamics and Materials Conference 6, 4057 – 4068.

Sherbourne, A., Bedair, O., 1993. Plate-stiffener assemblies in uniform compression. part ii: Postbuckling. Journal of Engineering Mechanics 119 (10), 1956–1972.

Shin, D. K., Griffin, O. H., Gürdal, Z., 1993. Postbuckling response of laminated plates under uniaxial compression. International Journal of Non-Linear Mechanics 28 (1), 95–115.

Stein, M., 1959. Loads and deformations of buckled rectangular plates. NASA Tech. Rep. R-40.

Wang, C.-T., 1952. Principle and application of complementary energy method for thin homogeneous and sandwich plates and shells with finite deflections. NACA, Report No. 2620.

Washizu, K., 1975. Variational Methods in Elasticity and Plasticity, Second Edition. Pergamon Press.

Wu, Z., Raju, G., , Weaver, P. M., 2012a. A comparison of variational, differential quadrature and approximate closed form solution methods for buckling of highly flexurally anisotropic laminates. Journal of Engineering Mechanics(accepted).

Wu, Z., Raju, G., Weaver, P. M., 2012b. Buckling analysis of vat plate using energy method. Collection of Technical Papers - 53rd AIAA/ASME Structures, Structural Dynamics and Materials Conference, 1–12.

Wu, Z., Weaver, P. M., Raju, G., Kim, B. C., 2012c. Buckling analysis and optimisation of variable angle tow composite plates. Thin-Walled Structures 60 (0), 163 – 172.

Yamaki, N., 1959. Postbuckling behavior of rectangular plates with small initial curvature loaded in edge compression. Journal of Applied Mechanics 26, 407414.

Zhang, Y., 1982. Buckling and postbuckling behaviour of generally layered composite panels. Ph.D. thesis, Imperial College, London.

A list of captions for the figures.

Figure 1: Boundary Conditions and Loading Cases.

Figure 2: Rayleigh-Ritz and FEA solutions of a square subjected to *case A*: (a) Normalised axial loads N_x/N_x^{iso} versus Normalised axial strain $\epsilon_x/\epsilon_x^{iso}$ (b) Normalised axial loads N_x/N_x^{iso} versus Normalized maximum transverse displacement w_{max}/h function.

Figure 3: Rayleigh-Ritz and FEA solutions of a square subjected to *case B*: (a) Normalised axial loads N_x/N_x^{iso} versus Normalised axial strain $\epsilon_x/\epsilon_x^{iso}$ (b) Normalised axial loads N_x/N_x^{iso} versus Normalised maximum transverse displacement w_{max}/h function.

Figure 4: Rayleigh-Ritz and FEA solutions of a square subjected to *case C*: (a) Normalised axial loads N_x/N_x^{iso} versus Normalised axial strain $\epsilon_x/\epsilon_x^{iso}$ (b) Normalised axial loads N_x/N_x^{iso} versus Normalised maximum transverse displacement w_{max}/h function.

Figure 5: Postbuckling and buckling performance of square simply-supported laminates under uniform displacement compression and the transverse edges are constrained (*case B*). (a) Relative stiffness K_r versus Normalised prebuckling stiffness (K_{pre}/K_{iso}) (b) Normalised postbuckling stiffness K_{post} versus Normalised prebuckling stiffness (c) Normalised overall stiffness K_o versus Normalised prebuckling stiffness (d) Normalised buckling load versus Nor-

malised prebuckling stiffness.

Figure 6: Postbuckling and buckling performance of square simply-supported laminates under uniform displacement compression and the transverse edges are free to move but keep straight (*case C*). (a) Relative stiffness K_r versus Normalised prebuckling stiffness (K_{pre}/K_{iso}) (b) Normalised postbuckling stiffness K_{post} versus Normalised prebuckling stiffness (c) Normalised overall stiffness K_o versus Normalised prebuckling stiffness (d) Normalised buckling load versus Normalised prebuckling stiffness.

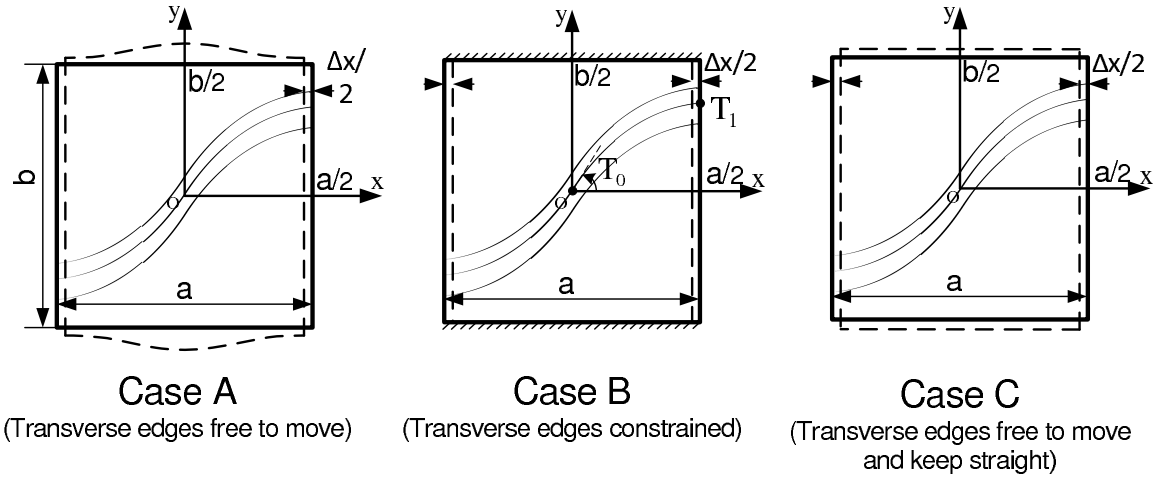

Figure 1: Boundary Conditions and Loading Cases

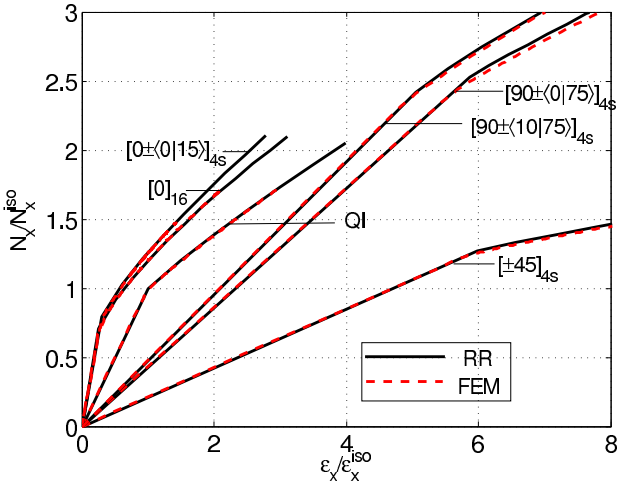

(a)

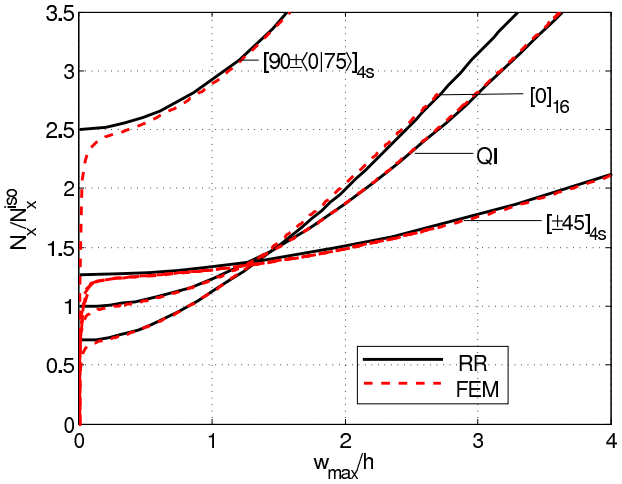

(b)

Figure 2: Rayleigh-Ritz and FEA solutions of a square simply-supported plate subjected to *case A*: (a) Normalised axial loads N_x/N_x^{iso} versus Normalised axial strain $\epsilon_x/\epsilon_x^{iso}$ (b) Normalised axial loads N_x/N_x^{iso} versus Normalized maximum transverse displacement w_{max}/h function.

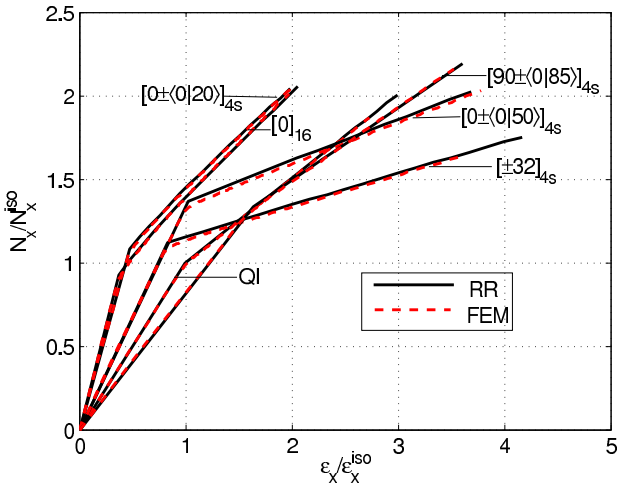

(a)

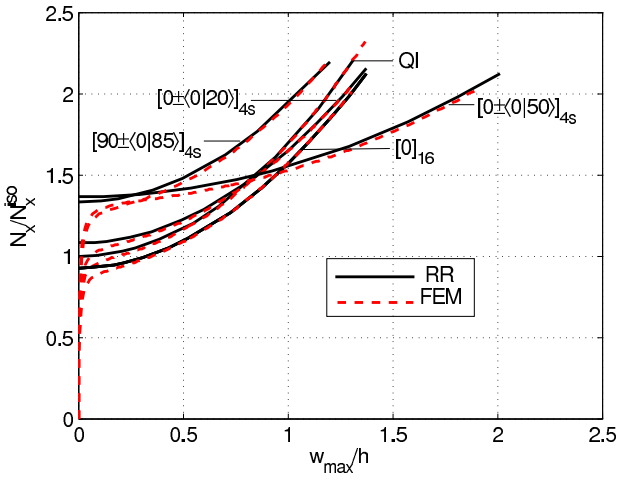

(b)

Figure 3: Rayleigh-Ritz and FEA solutions of a square simply-supported plate subjected to *case B*: (a) Normalised axial loads N_x/N_x^{iso} versus Normalised axial strain $\epsilon_x/\epsilon_x^{iso}$ (b) Normalised axial loads N_x/N_x^{iso} versus Normalised maximum transverse displacement w_{max}/h function.

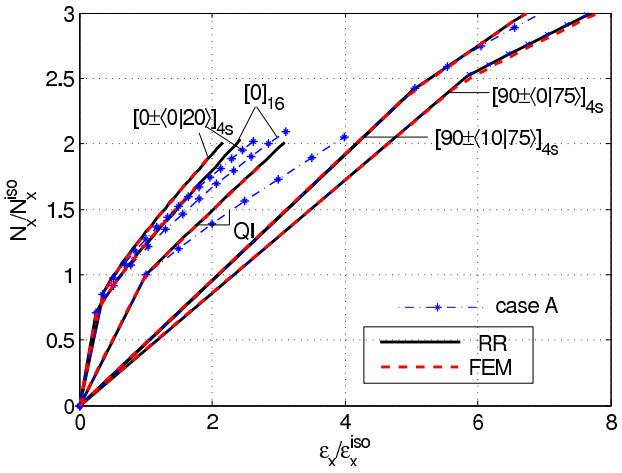

(a)

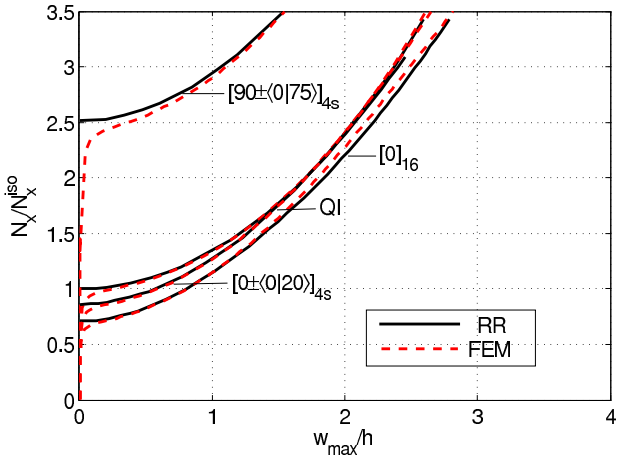

(b)

Figure 4: Rayleigh-Ritz and FEA solutions of a square simply-supported plate subjected to *case C*: (a) Normalised axial loads N_x/N_x^{iso} versus Normalised axial strain $\epsilon_x/\epsilon_x^{iso}$ (b) Normalised axial loads N_x/N_x^{iso} versus Normalised maximum transverse displacement w_{max}/h function.

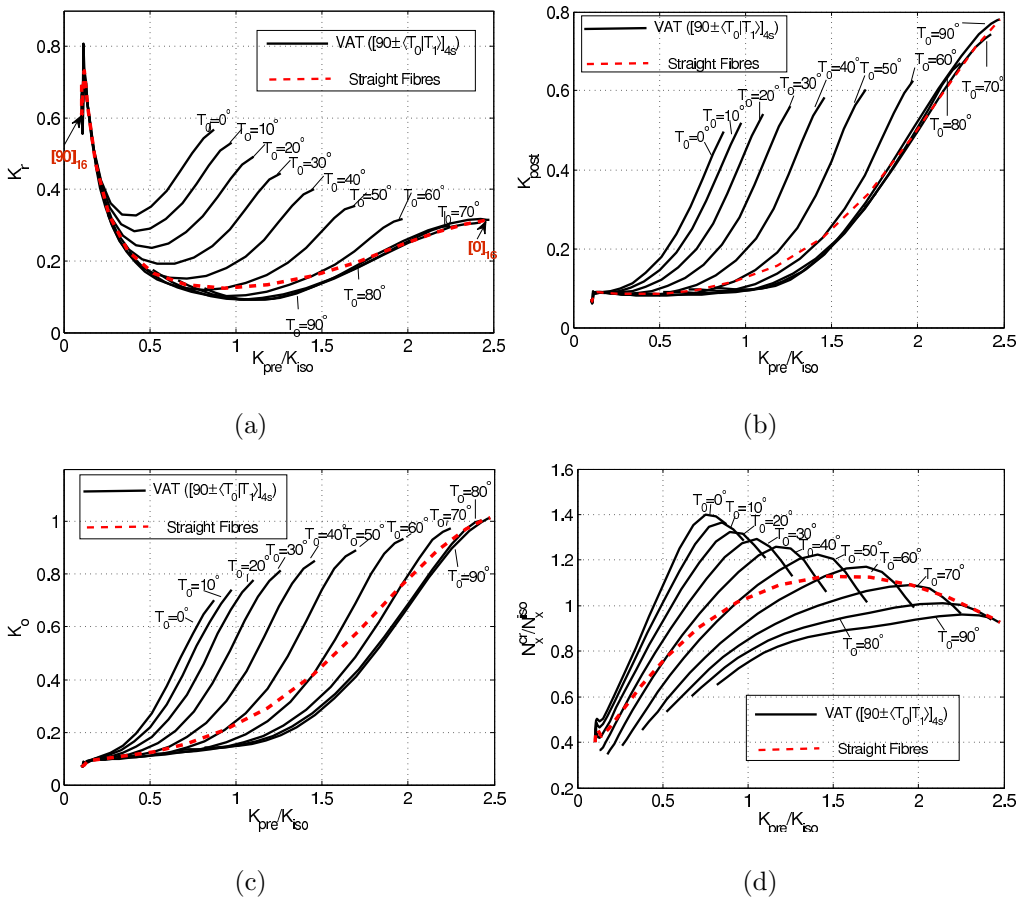

Figure 5: Postbuckling and buckling performance of square simply-supported laminates under uniform displacement compression and the transverse edges are constrained (*case B*). (a) Relative stiffness K_r versus Normalised prebuckling stiffness (K_{pre}/K_{iso}) (b) Normalised postbuckling stiffness K_{post} versus Normalised prebuckling stiffness (c) Normalised overall stiffness K_o versus Normalised prebuckling stiffness (d) Normalised buckling load versus Normalised prebuckling stiffness

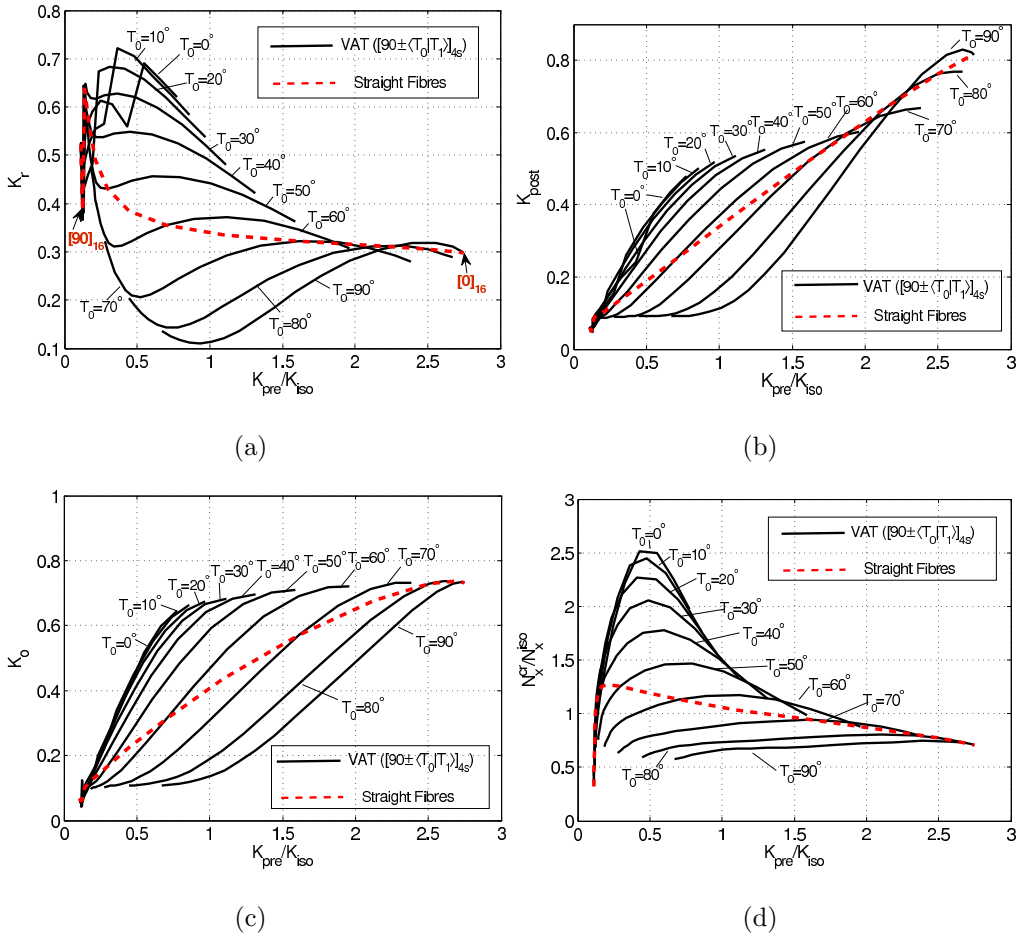

Figure 6: Postbuckling and buckling performance of square simply-supported laminates under uniform displacement compression and the transverse edges are free to move but keep straight (*case C*). (a) Relative stiffness K_r versus Normalised prebuckling stiffness (K_{pre}/K_{iso}) (b) Normalised postbuckling stiffness K_{post} versus Normalised prebuckling stiffness (c) Normalised overall stiffness K_o versus Normalised prebuckling stiffness (d) Normalised buckling load versus Normalised prebuckling stiffness